Supporting Information

# Rapid and convenient oxidative release of thiol-conjugated forms of microcystins for chemical analysis

Christopher O. Miles[1,2,*]

[1]Norwegian Veterinary Institute, P. O. Box 750 Sentrum, N-0106 Oslo, Norway
[2]National Research Council, 1411 Oxford Street, Halifax, NS, B3H 3Z1, Canada

*Author to whom correspondence should be addressed:
Phone +1 (902) 426-7263
Fax +1 (902) 426 9413
Email chris.miles@nrc.ca

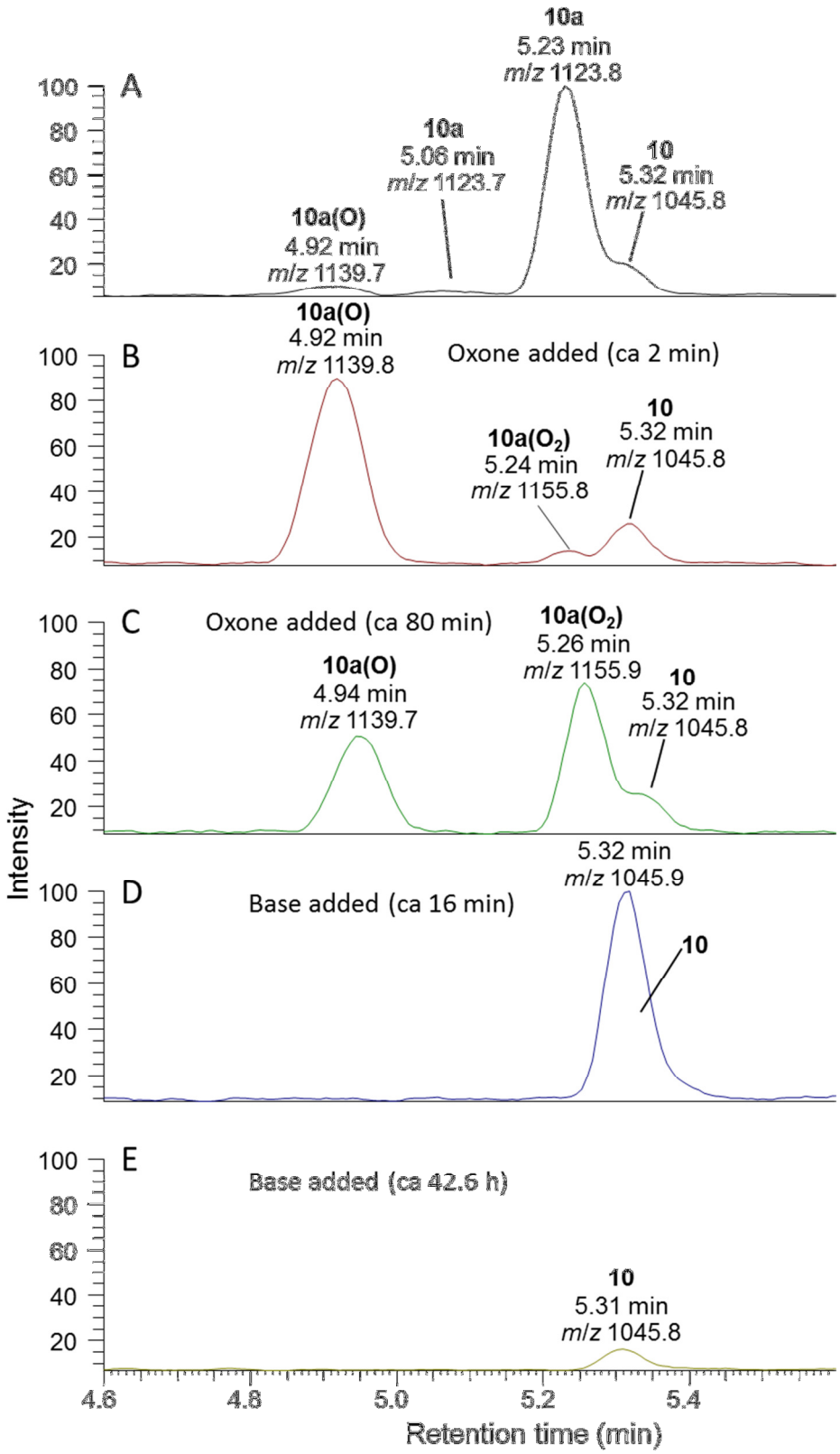


**Figure S1.** LC–MS analysis of step-wise oxidation with Oxone, followed by addition of carbonate buffer. (experiment A, #2). The rate of oxidation of sulfide **10a** to sulfoxide **10a(O)** was too fast to measure with LC–MS[2] ($t_{½}$ < 5 min). However oxidation of sulfoxide **10a(O)** to sulfone **10a(O$_2$)** followed first-order kinetics with $t_{½}$ 68 min. Chromatograms are at the same vertical scale, corrected for dilution by addition of reagents, extracted at *m*/*z* for $[M+H]^+$ of **10**, **10a**, **10a(O)** and **10(O$_2$)**.

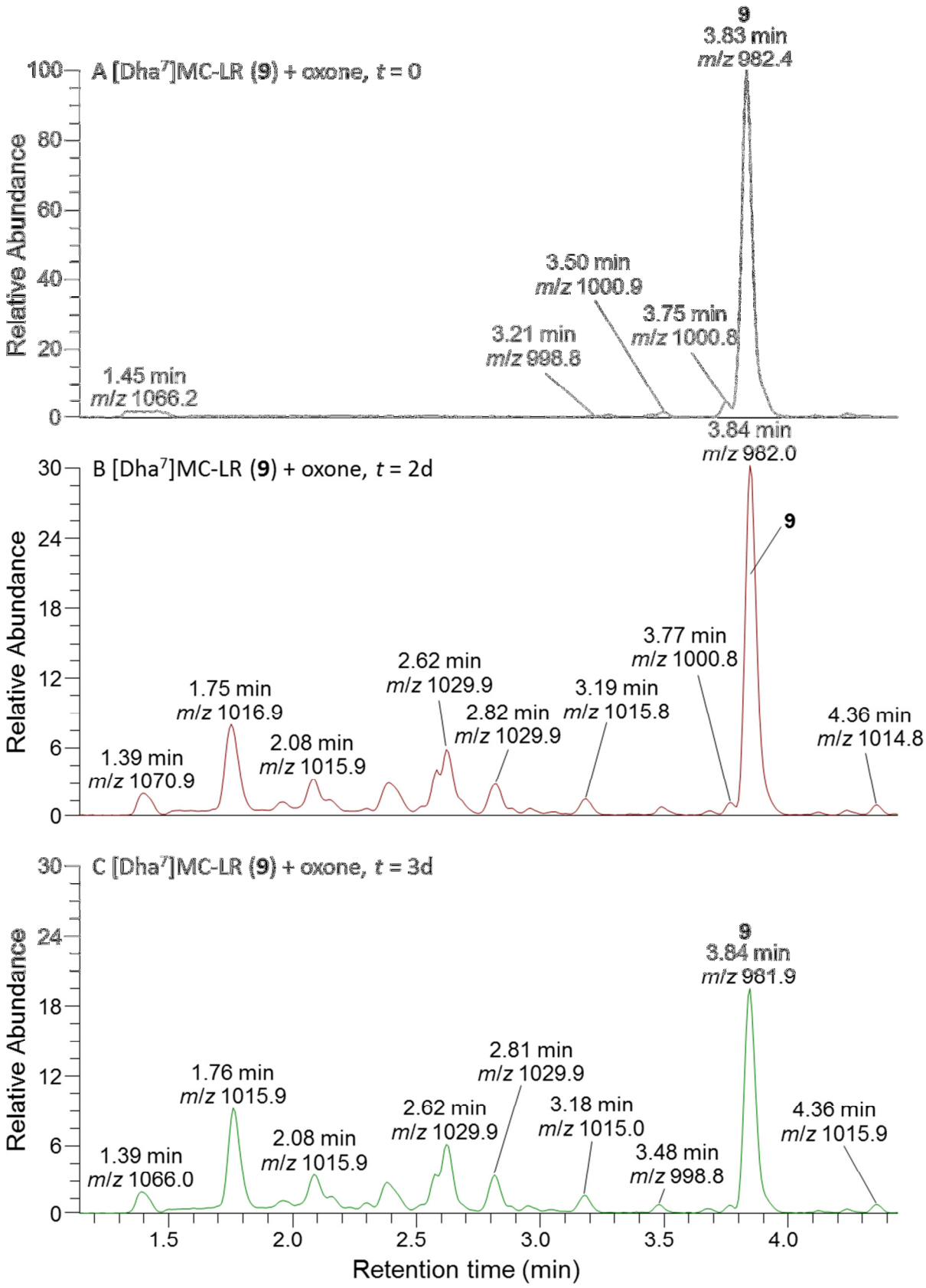


**Figure S2.** LC–MS analysis of treatment of [Dha$^7$]MC-LR (**9**) in MeOH–$H_2O$ with Oxone, showing the reduction in intensity of **9** and production of oxidized microcystin degradation products (experiment A, #3). Chromatograms are at the same absolute vertical scale, but with an expansion (showing 0–30%) for oxidized samples.

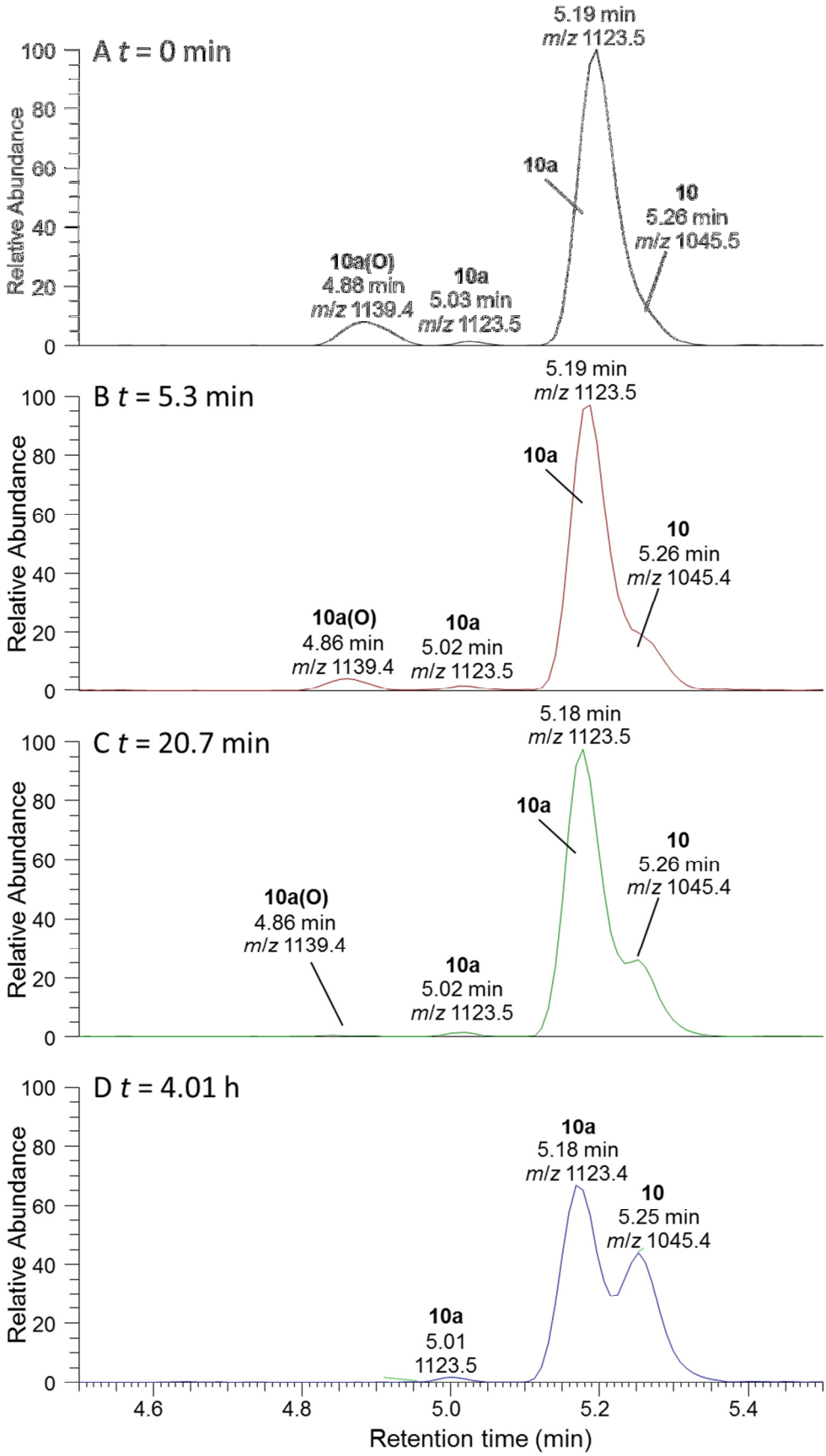


**Figure S3.** LC–MS$^2$ analysis of the first 4 h of deconjugation of **10a** contaminated with ca 15% of its sulfoxide (**10a(O)**) (experiment B). Chromatograms are at the same vertical scale, extracted at *m/z* for $[M+H]^+$ of **10**, **10a**, and **10a(O)**.

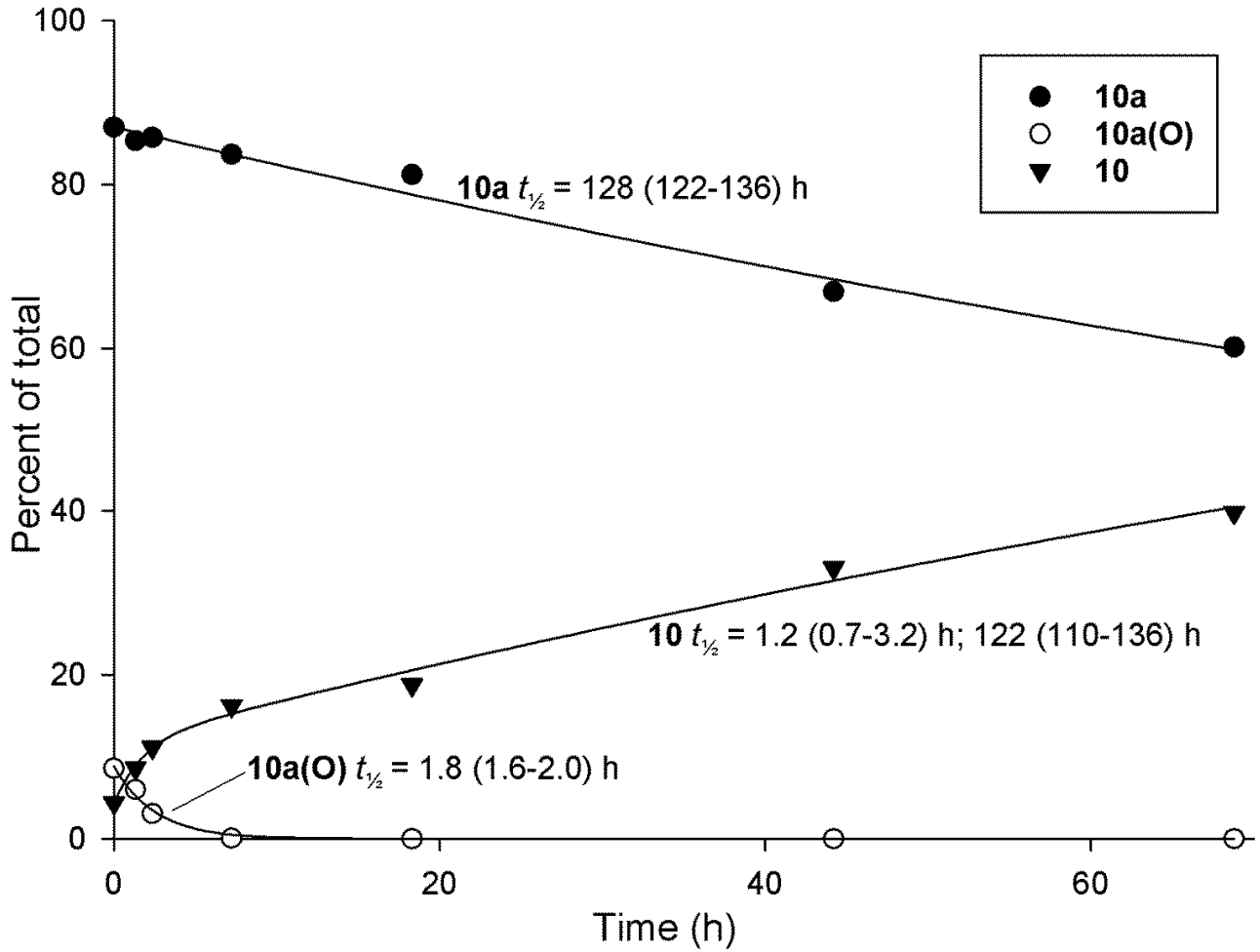


**Figure S4**. Reanalysis of LC–$MS^2$ data for the deconjugation of **10a** and production of **10** at pH 9.2 with $Me_2SO$,[1] but including the presence of sulfoxide-**10a(O)**. Concentrations of **10a** and **10a(O)** are fitted to 2-parameter exponential decay curves, and the concentration of **10** is fitted to a 5-parameter exponential increase to a maximum (resulting in two rate constants). Values in parentheses show $t_{½}$ ± SE.

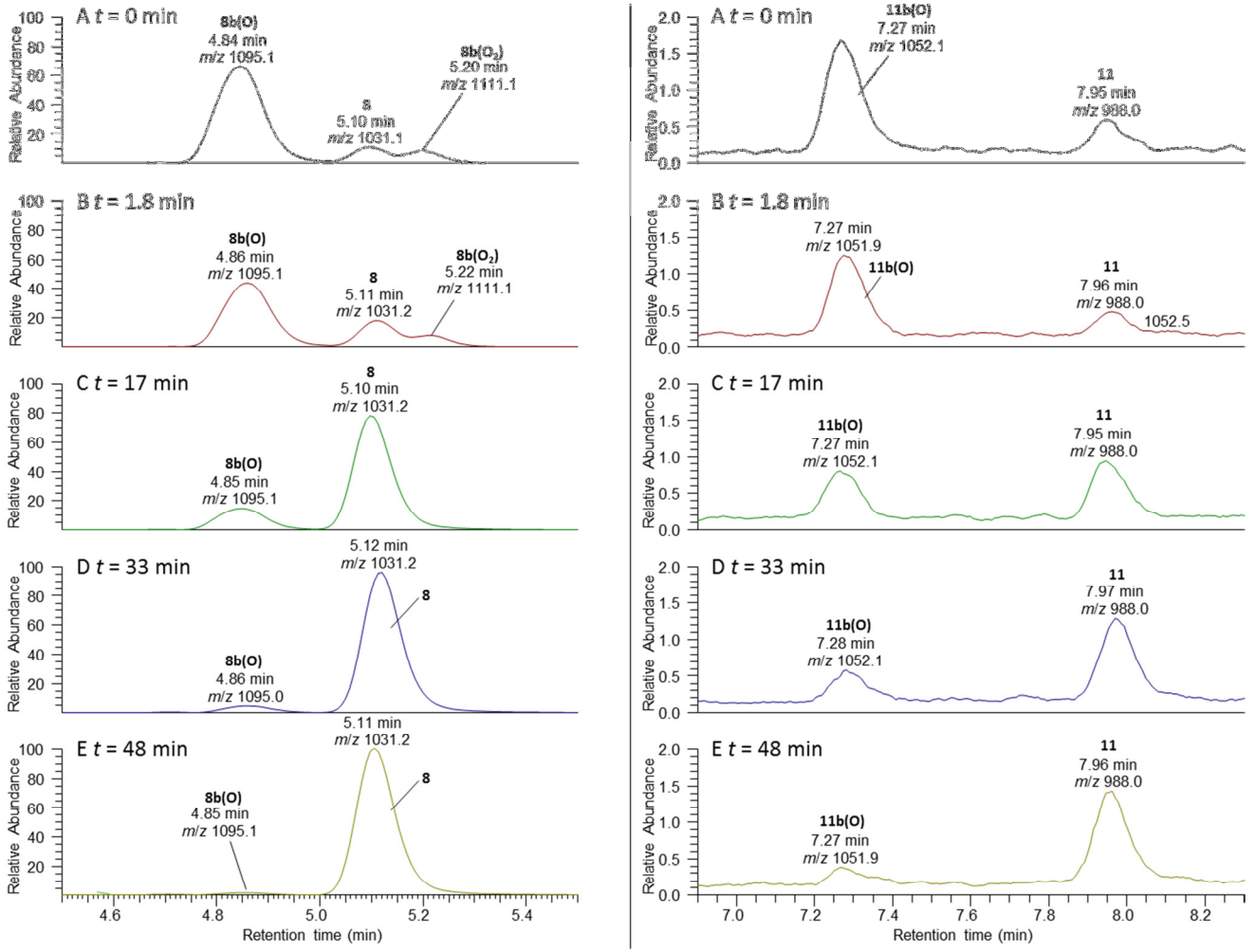


**Figure S5.** LC–MS analysis of the base-catalyzed deconjugation of methanethiol-conjugate **8b** via its sulfoxide (**8b(O)**) and sulfone (**8b($O_2$)**) (left panels) after treatment with $H_2O_2$ followed by SPE (experiment C). Note the presence of a small amount of **11b(O)** in the reaction mixture (panels on right), which was deconjugated in a similar manner to **8b(O)** but at a slower rate. Only trace levels of **11b($O_2$)** were present. Chromatograms are extracted at *m/z* for $[M+H]^+$ of the marked compounds, and are presented at the same absolute vertical scale corrected for dilution by addition of reagents, but with an expansion (showing 0–2%) for the region showing **11b(O)** and **11b**.

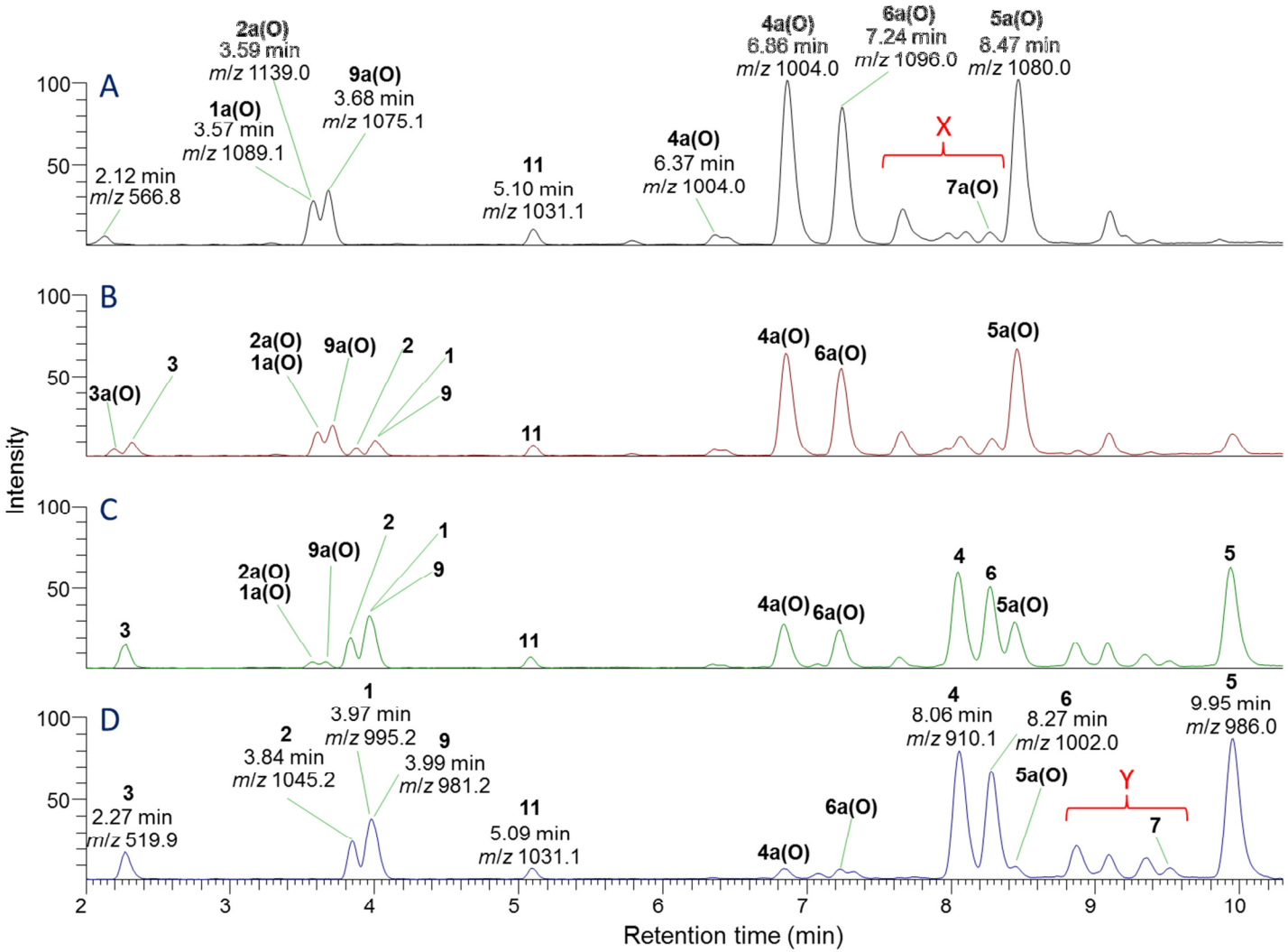


**Figure S6.** LC–$MS^2$ analysis of the base-catalyzed deconjugation of sulfoxides **1a(O)**–**7a(O)** and **9a(O)**, produced by $H_2O_2$ oxidation of the mercaptoethanol adducts of a mixture of MC followed by SPE separation (experiment C). The regions marked X and Y contain peaks arising from oxidation of the mercaptoethanol adduct of MC-LW (**7a**), and expansions are shown in Figure S7.

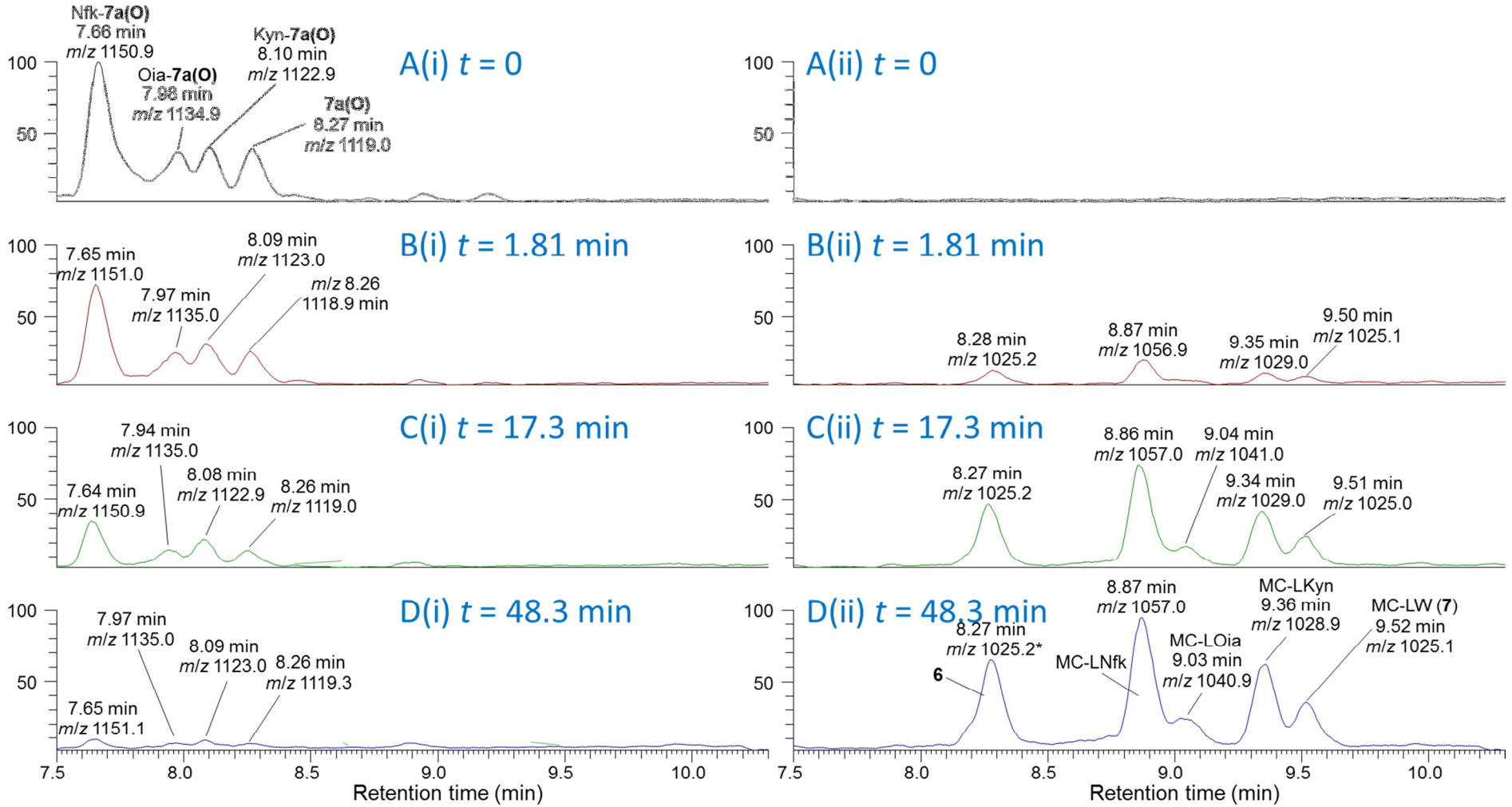


**Figure S7.** Expansion from LC-MS$^2$ analysis (Figure S6) showing the deconjugation of the sulfoxides of the mercaptoethanol adduct of MC-LW and its oxidation products at various times after addition of carbonate buffer (experiment C). Chromatograms on the left are extracted for *m/z* for $[M+H]^+$ of **7a(O)** and its Oia-, Nfk- and Kyn-derivatives, while those on the right are extracted for *m/z* for $[M+H]^+$ of **7a** and its Oia-, Nfk- and Kyn-derivatives. All chromatograms are shown with the same absolute vertical scale.

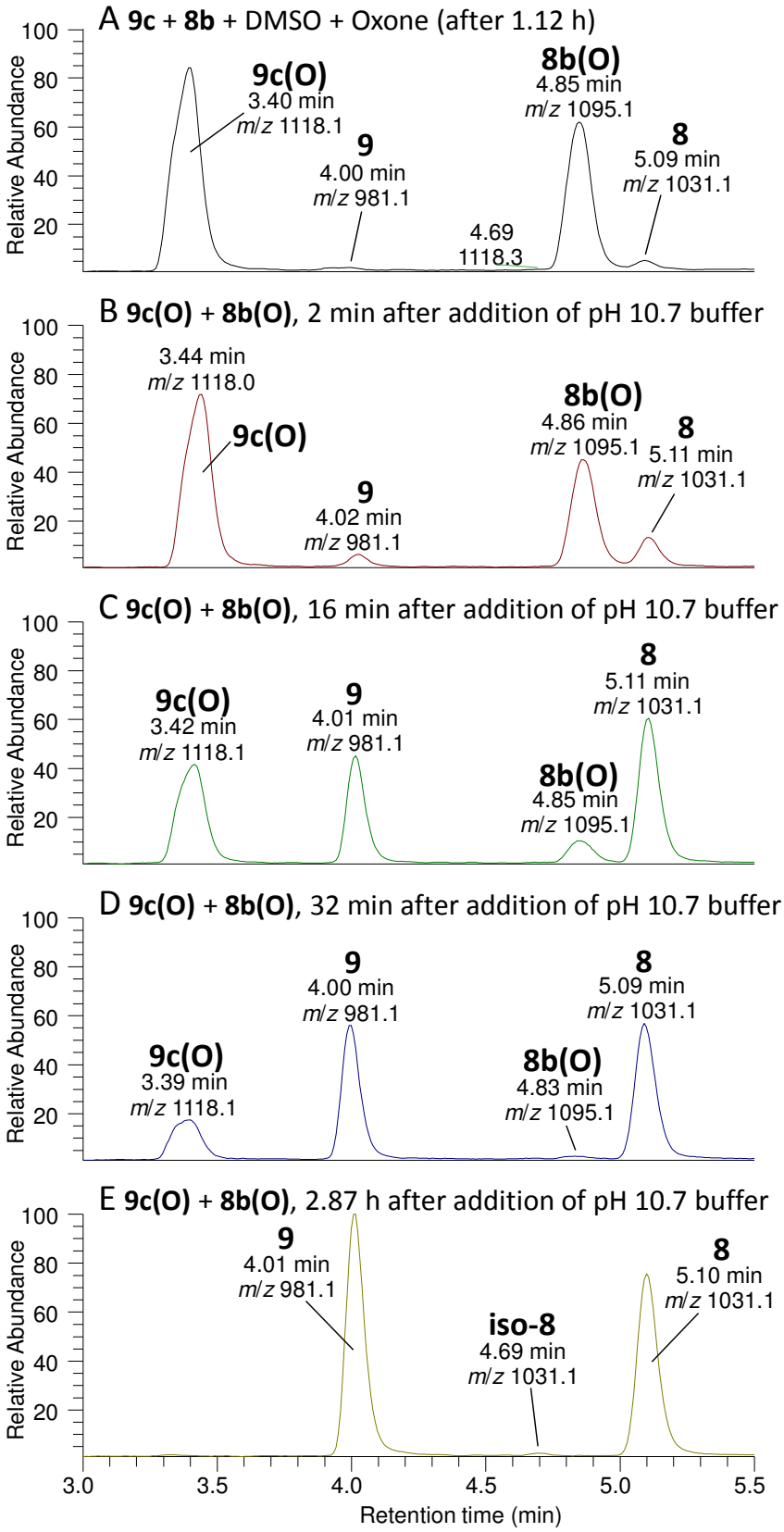


**Figure S8.** LC-MS$^2$ chromatograms of the deconjugation of the sulfoxides of Cys-conjugate **9c** and MeSH-conjugate **8b** (experiment E). All chromatograms are extracted for *m*/*z* for ($[M+H]^+$ + $[M+2H]^{2+}$) of **8**, **8b**, **8b(O)**, **9**, **9c**, and **9c(O)** and are shown at the same absolute vertical scale. Peaks are labelled with retention time and *m*/*z* for $[M+H]^+$.

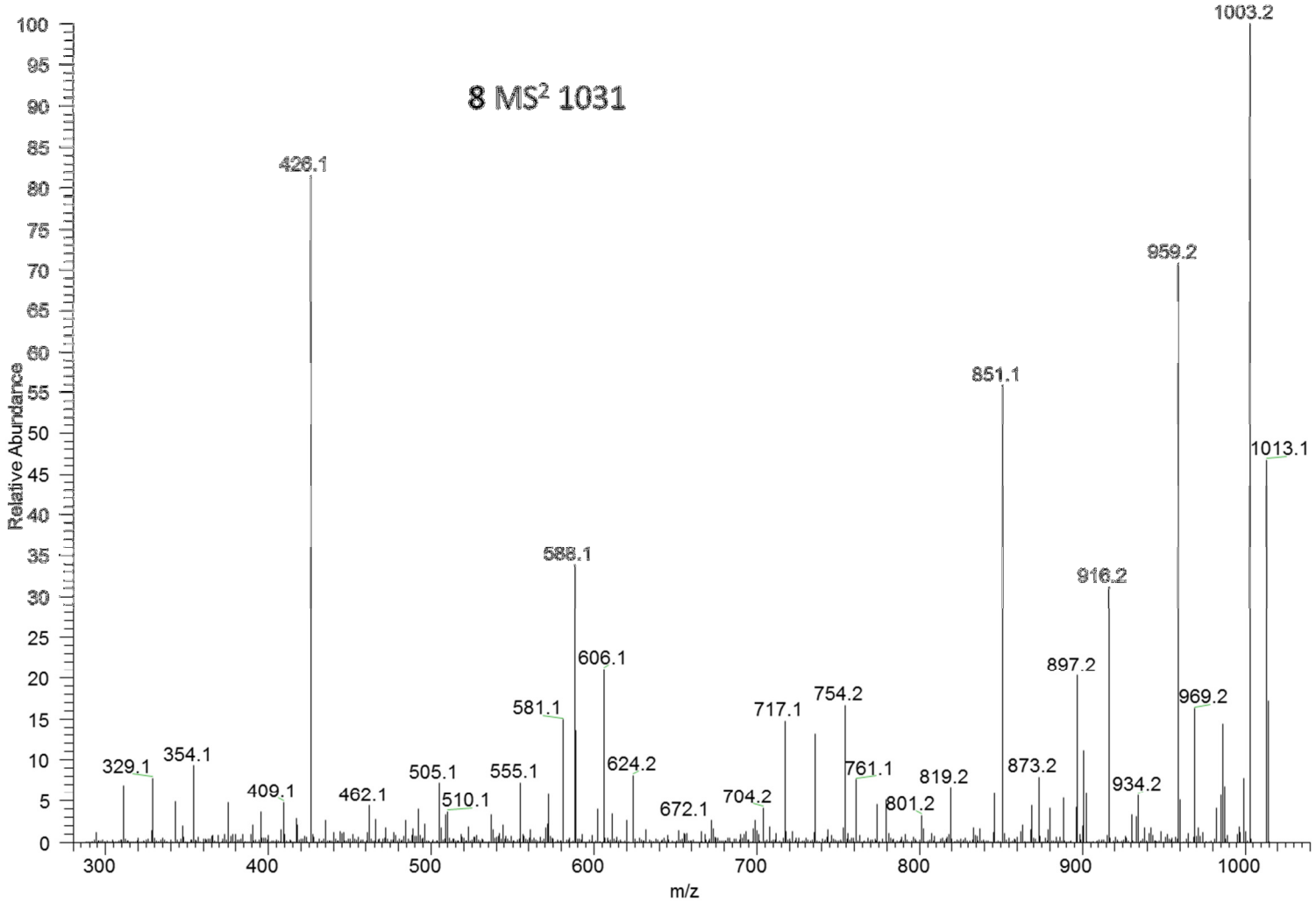


**Figure S9.** LC–$MS^2$ spectrum of $[M+H]^+$ of [$Asp^3$]MC-RY (**8**) at *m/z* 1031.2.

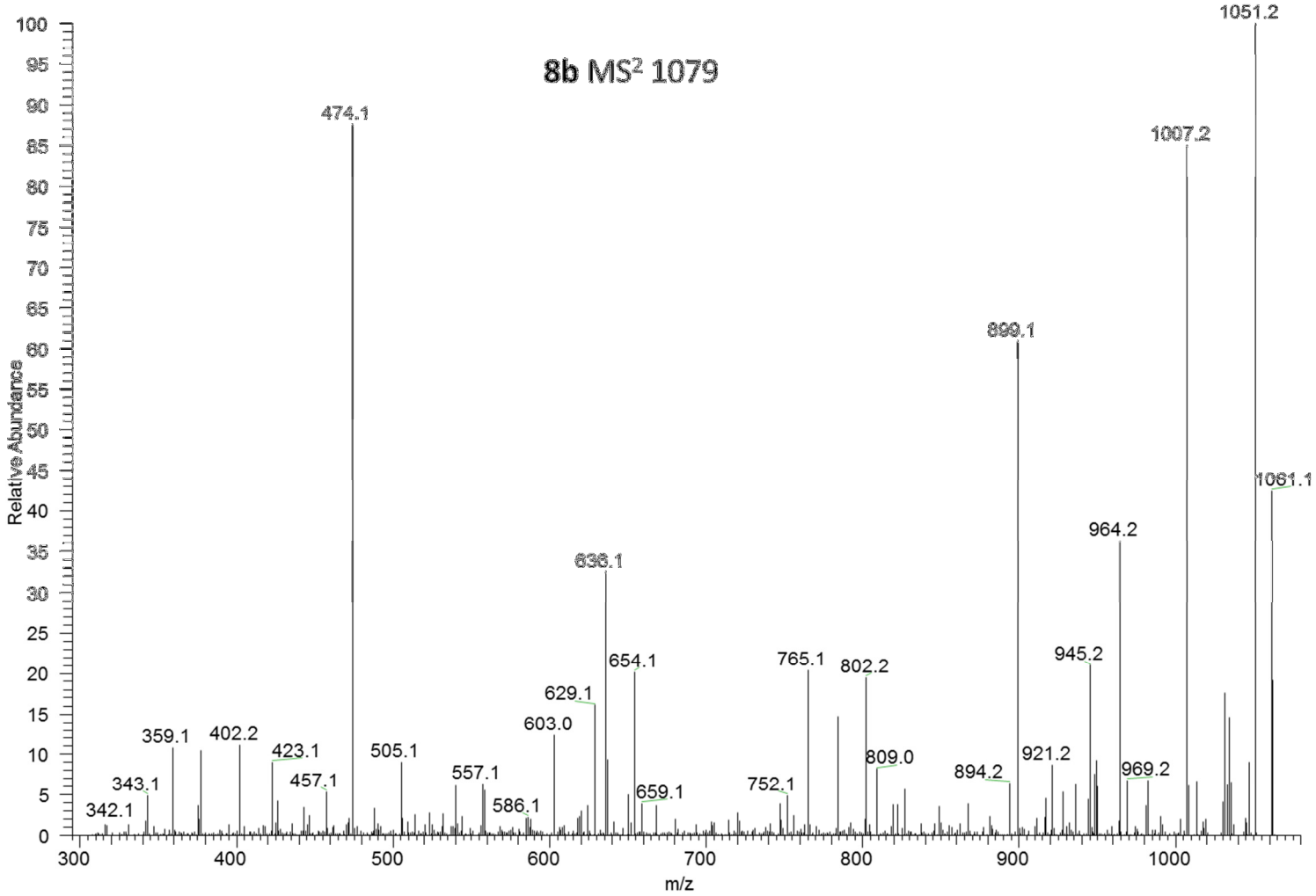


**Figure S10.** LC–$MS^2$ spectrum of $[M+H]^+$ of the methanethiol adduct of [$Asp^3$]MC-RY (**8b**) at *m/z* 1079.2.

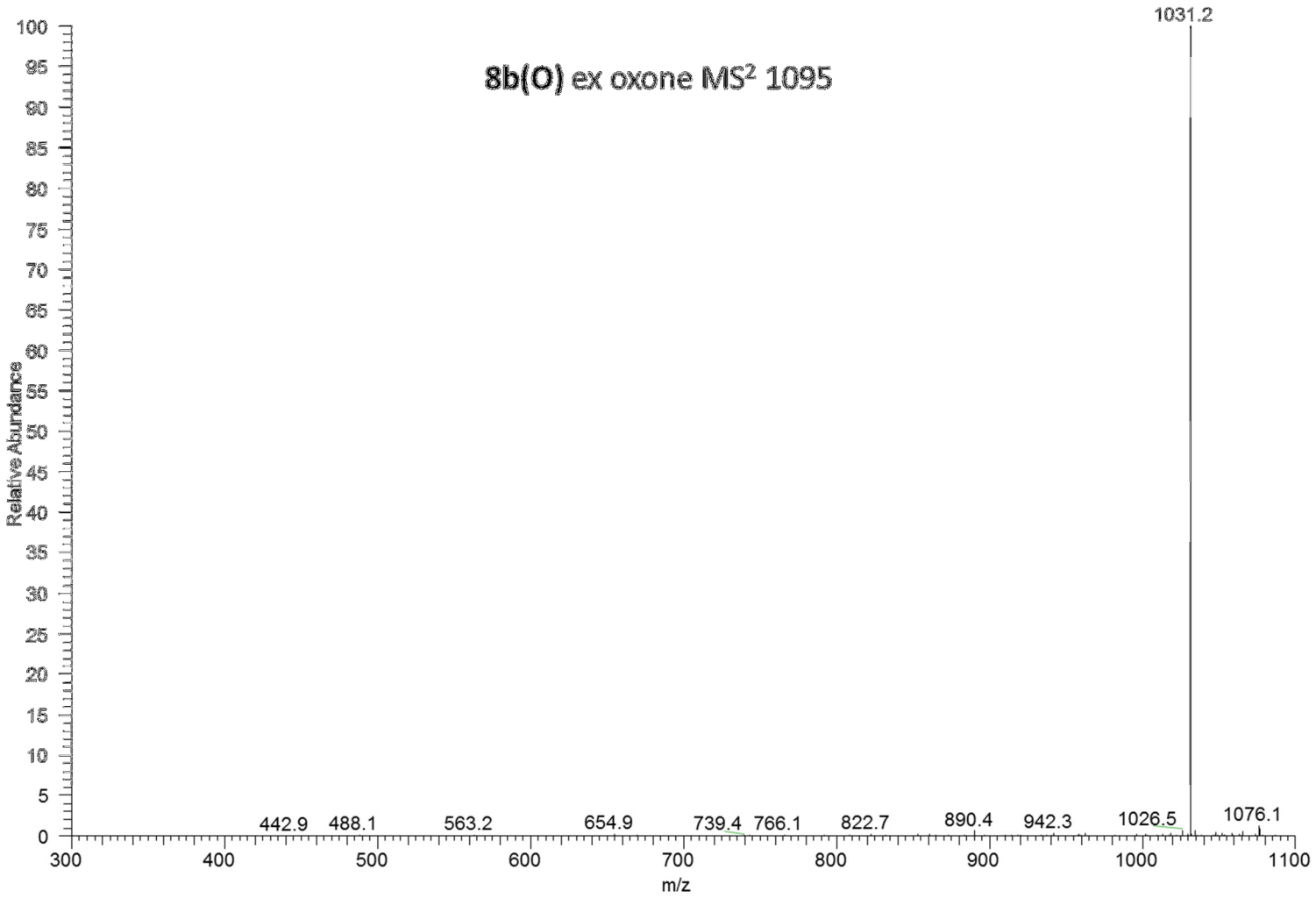


**Figure S11.** LC–$MS^2$ spectrum of $[M+H]^+$ of the sulfoxide of the methanethiol adduct of [$Asp^3$]MC-RY (**8b(O)**) at *m/z* 1095.2, produced by oxidation of **8b** with Oxone.

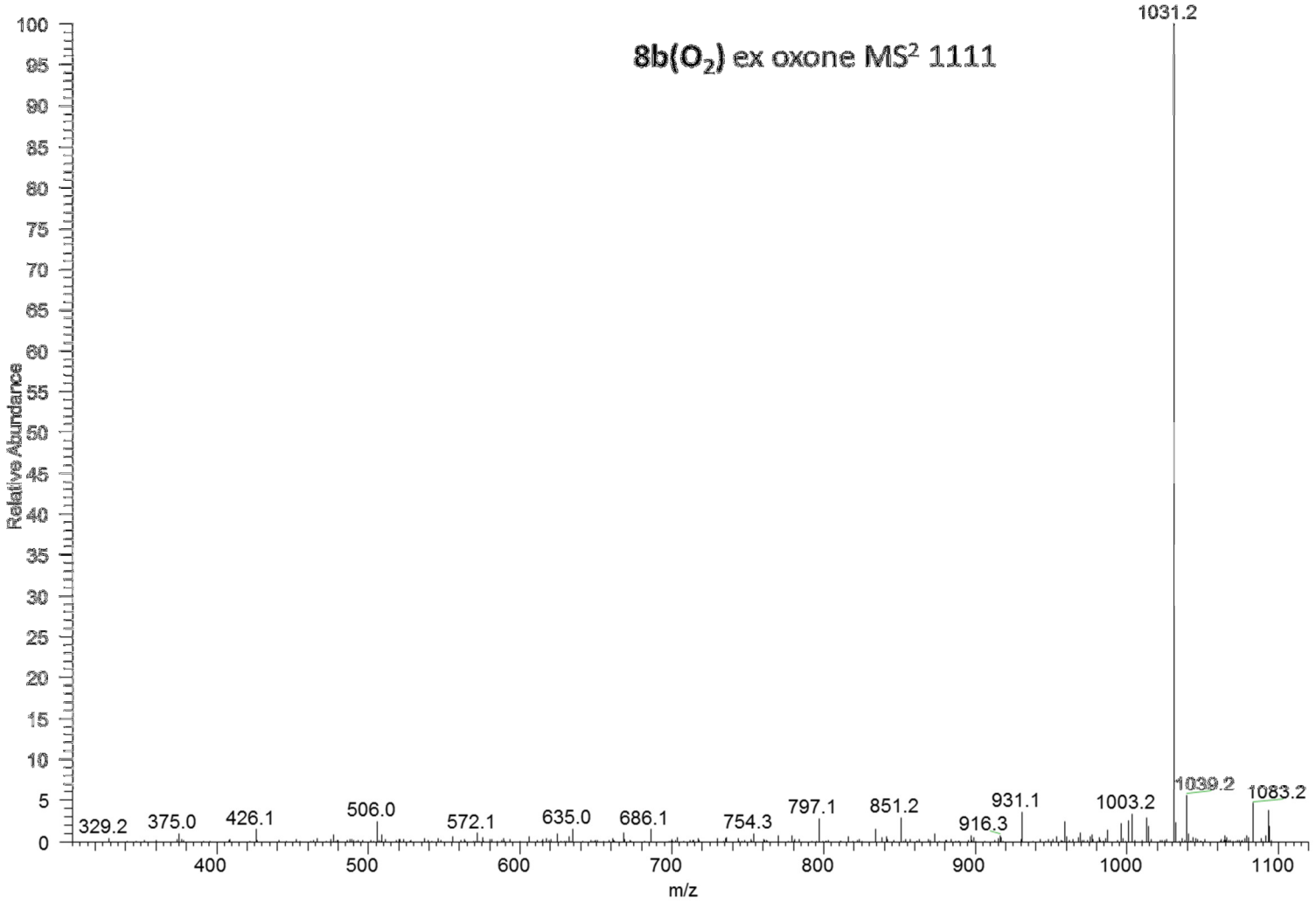


**Figure S12.** LC–$MS^2$ spectrum of $[M+H]^+$ of the sulfone of the methanethiol adduct of [$Asp^3$]MC-RY (**8b($O_2$)**) at *m/z* 1111.2, produced by oxidation of **8b** with Oxone.

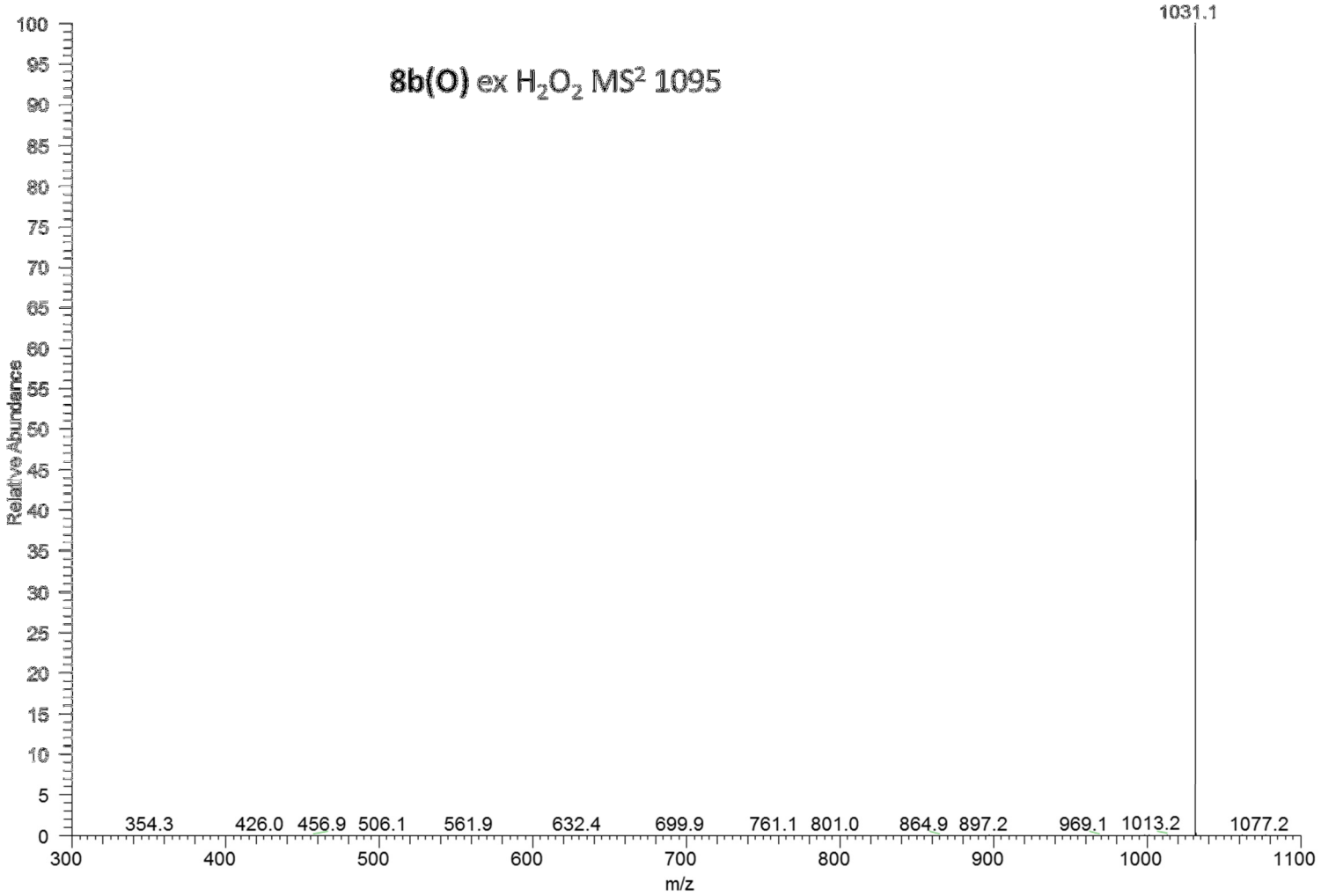


**Figure S13.** LC–$MS^2$ spectrum of $[M+H]^+$ of the sulfoxide of the methanethiol adduct of [$Asp^3$]MC-RY (**8b(O)**) at *m/z* 1095.2, produced by oxidation of **8b** with $H_2O_2$.

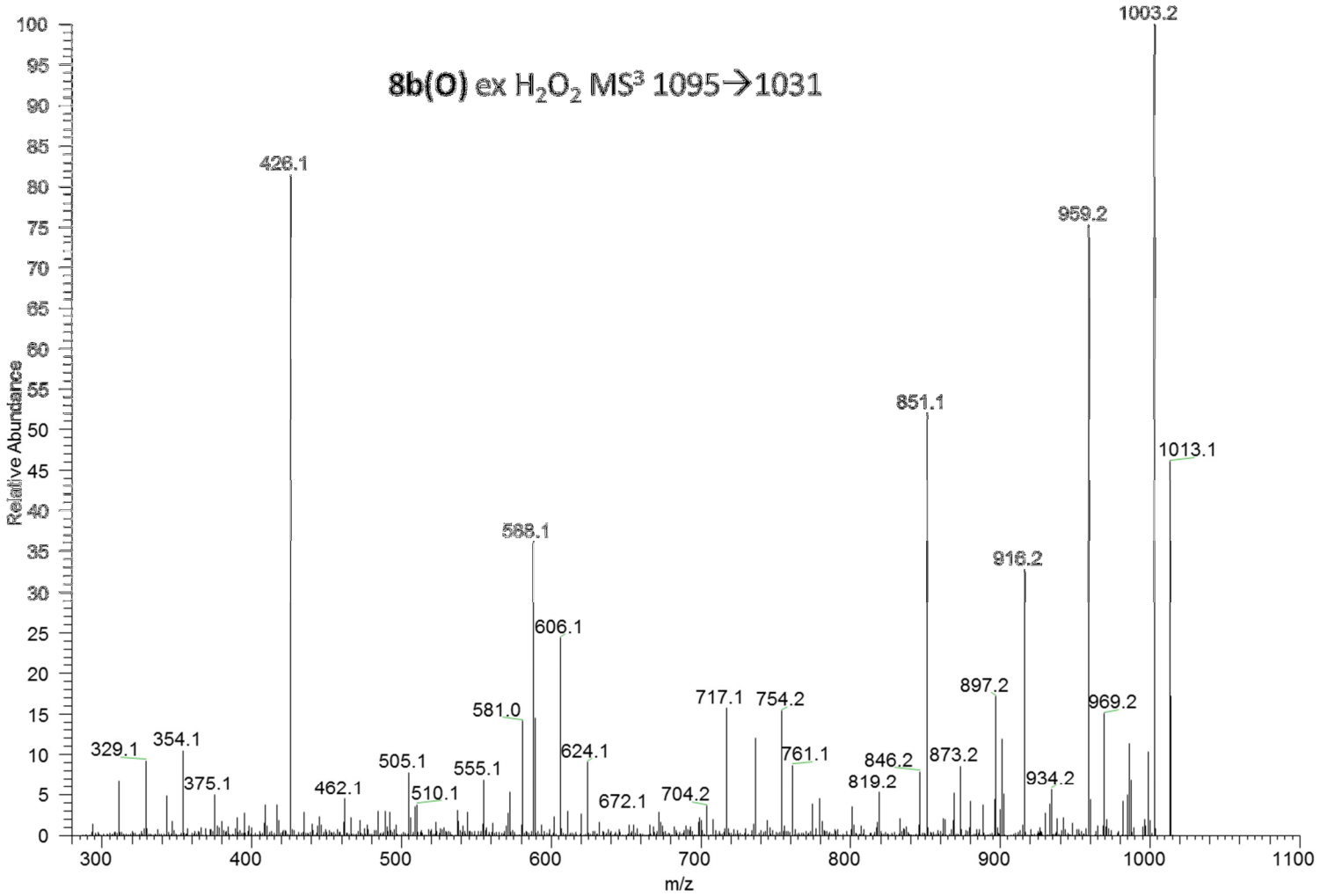


**Figure S14.** LC–$MS^3$ spectrum of $[M+H]^+$ of the sulfoxide of the methanethiol adduct of [$Asp^3$]MC-RY (**8b(O)**) at *m/z* 1095.2→1031.2, produced by oxidation of **8b** with $H_2O_2$.

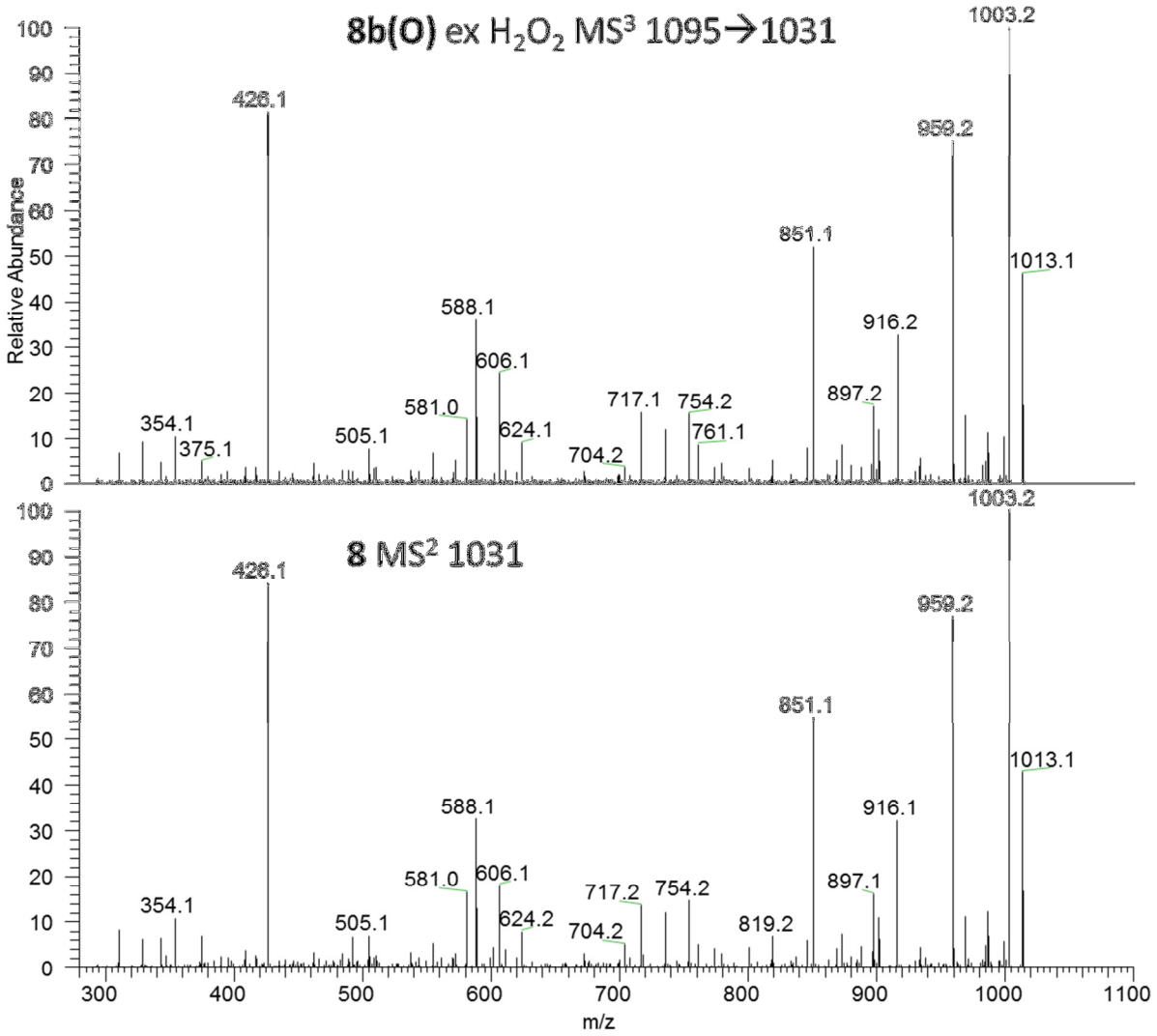


**Figure S15.** Top, LC–$MS^3$ spectrum of $[M+H]^+$ of the sulfoxide of the methanethiol adduct of [$Asp^3$]MC-RY (**8b(O)**) at *m/z* 1095.2→1031.2, produced by oxidation of **8b** with $H_2O_2$; bottom, LC–$MS^2$ spectrum of $[M+H]^+$ of [$Asp^3$]MC-RY (**8**) at *m/z* 1031.2.

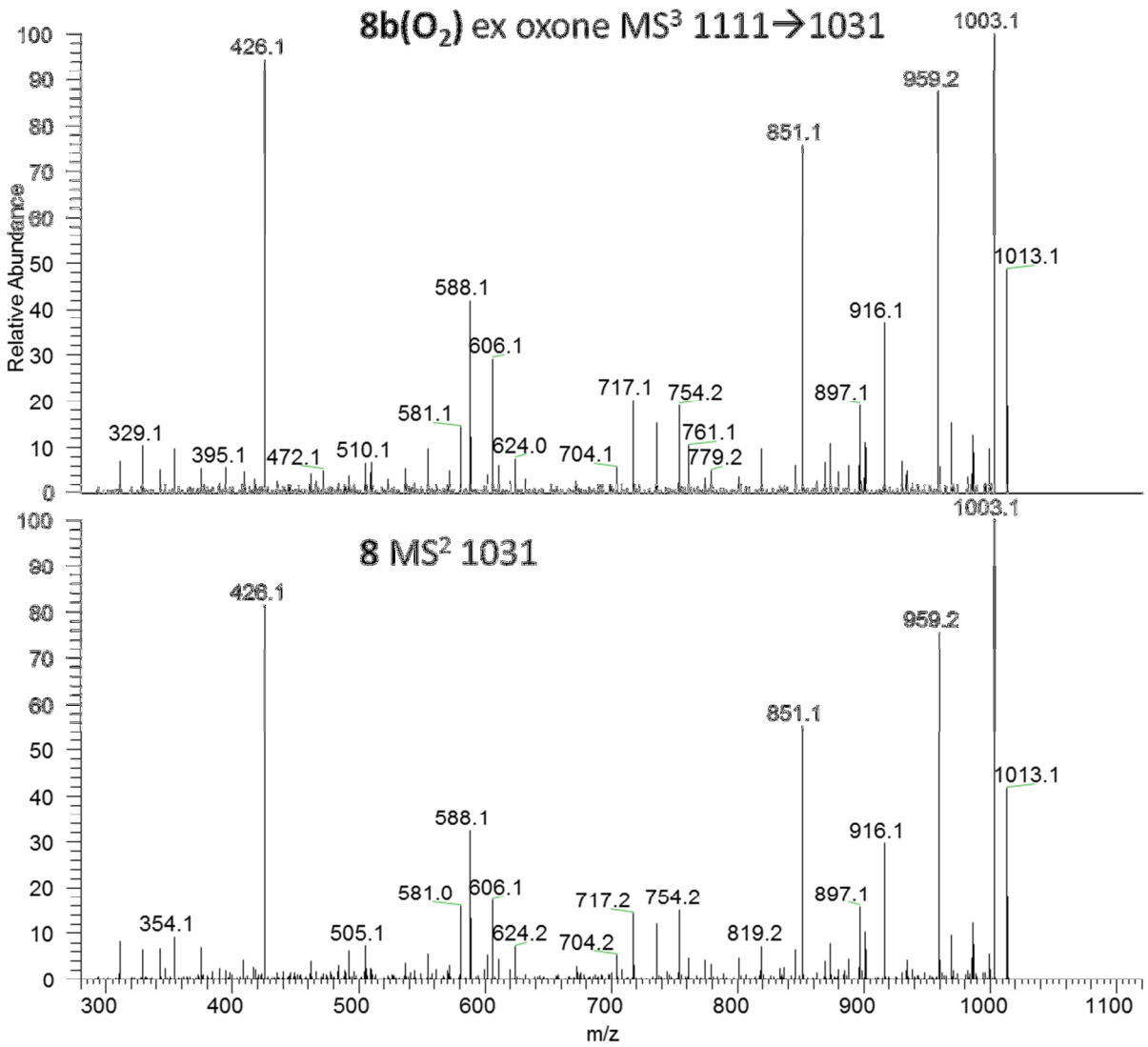


**Figure S16.** Top, LC–$MS^3$ spectrum of $[M+H]^+$ of the sulfone of the methanethiol adduct of [$Asp^3$]MC-RY (**8b($O_2$)**) at *m/z* 1111.2→1031.2, produced by oxidation of **8b** with Oxone; bottom, LC–$MS^2$ spectrum of $[M+H]^+$ of [$Asp^3$]MC-RY (**8**) at *m/z* 1031.2.

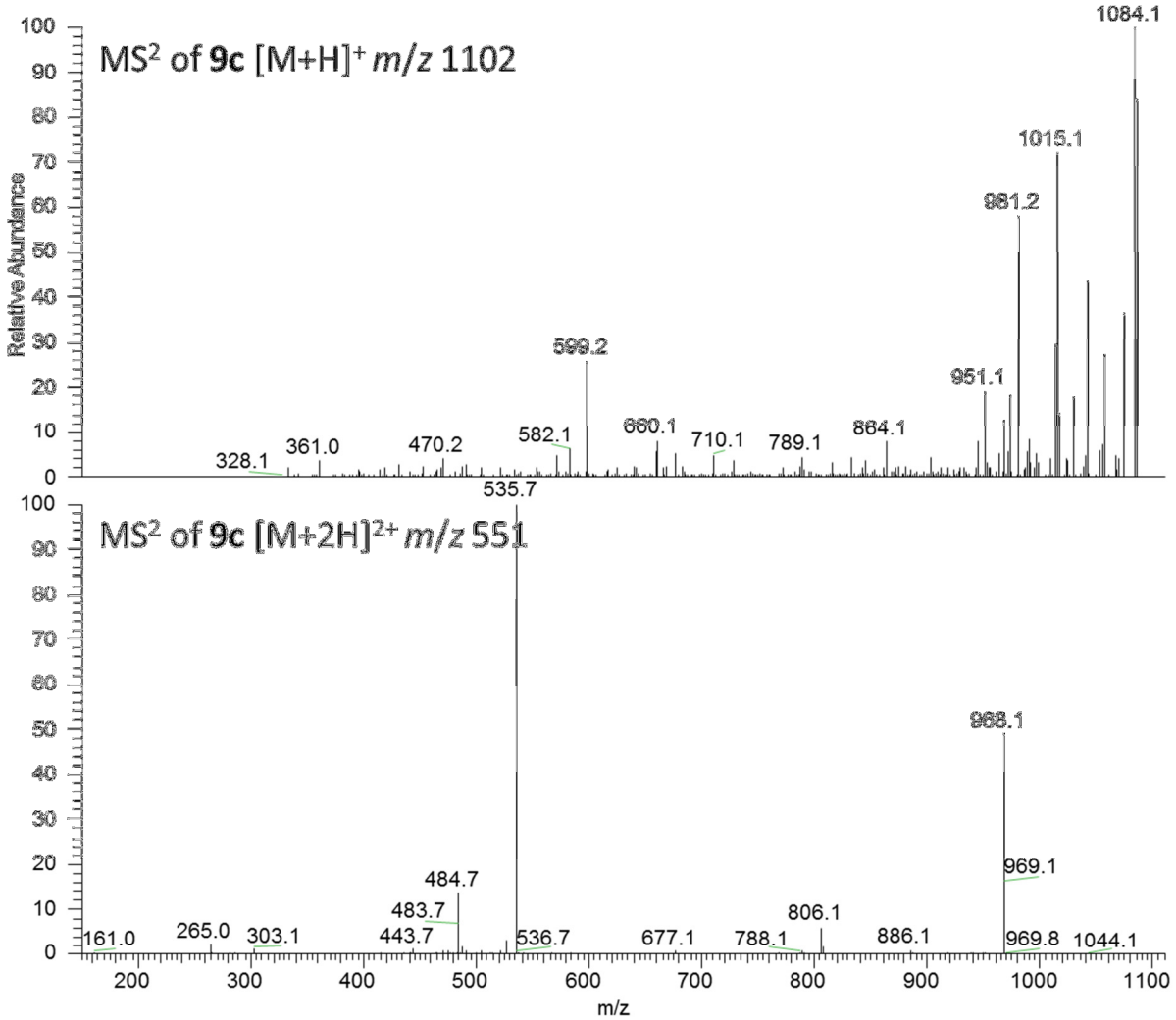


**Figure S17.** Top, LC–$MS^2$ spectrum of $[M+H]^+$ of the Cys adduct of [$Dha^7$]MC-LR (**9c**) at *m/z* 1102.1; bottom, LC–$MS^2$ spectrum of $[M+2H]^{2+}$ of the Cys adduct of [$Dha^7$]MC-LR (**9c**) at *m/z* 551.8.

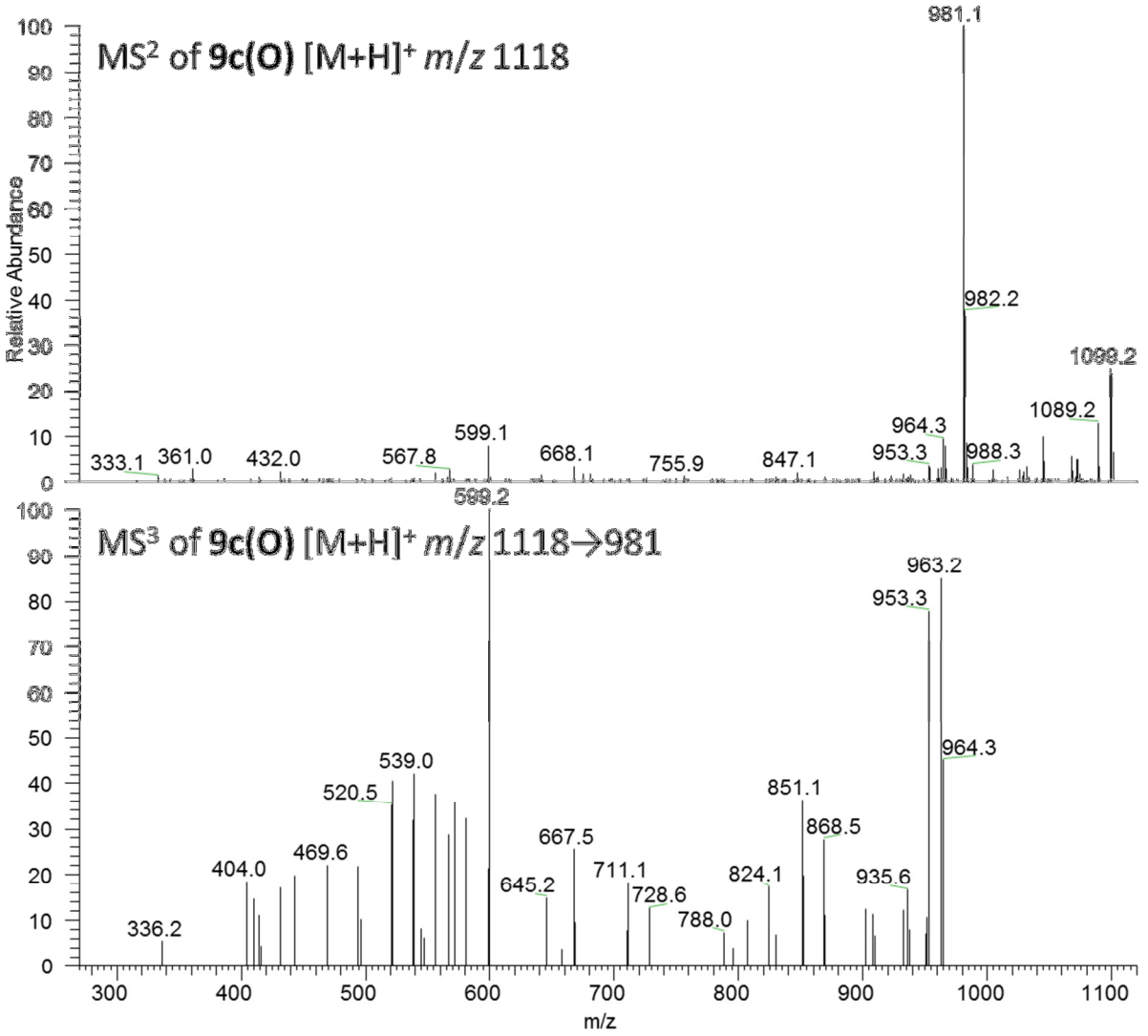


**Figure S18.** Top, LC–MS$^2$ spectrum of [M+H]$^+$ of the sulfoxide of the Cys adduct of [Dha$^7$]MC-LR (**9c(O)**) at *m/z* 1118.0; bottom, LC–MS$^3$ spectrum of [M+H]$^+$ of the sulfoxide of the Cys adduct of [Dha$^7$]MC-LR (**9c(O)**) at *m/z* 1118.0→981.1 (note, low signal-to-noise).

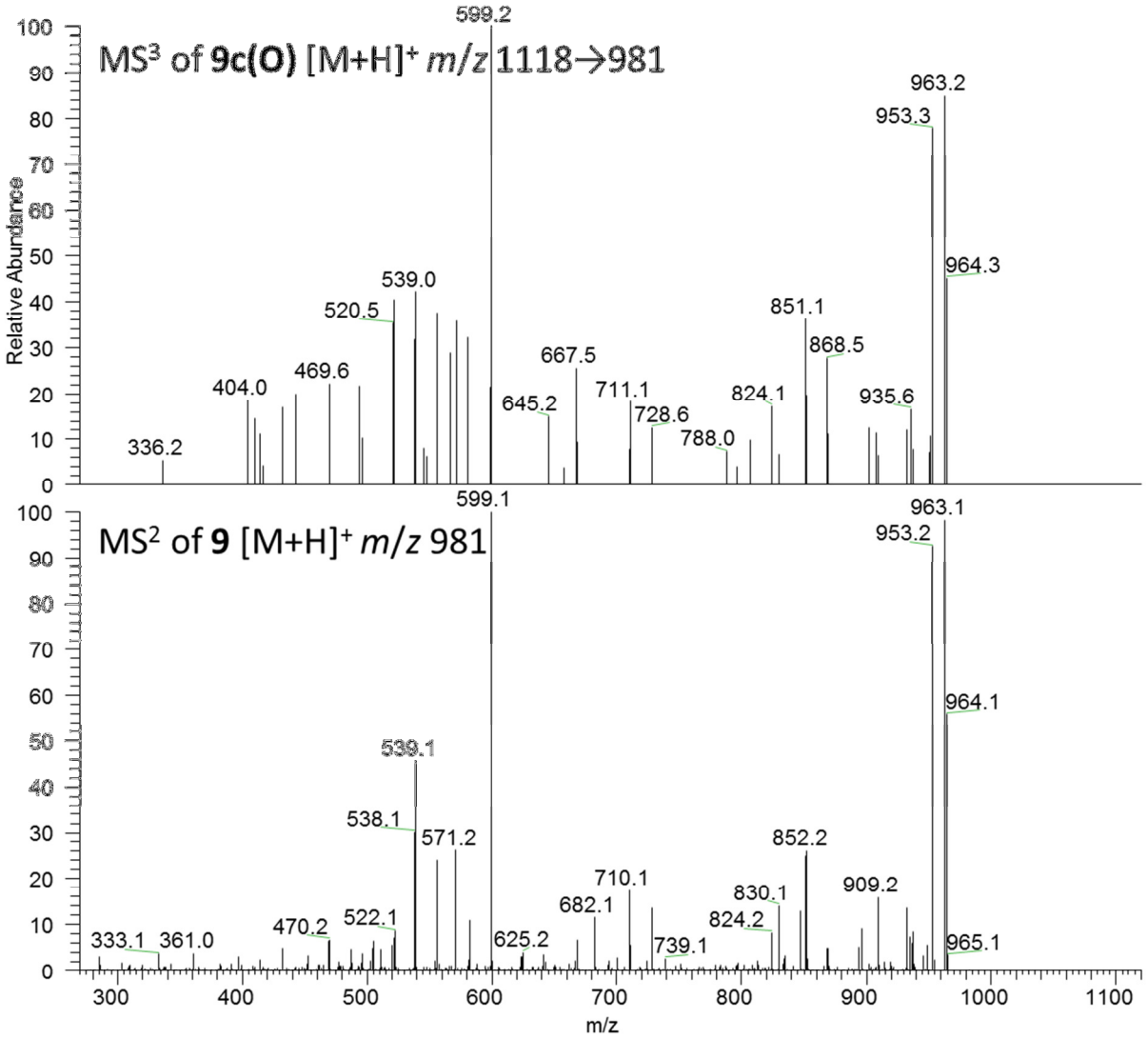


**Figure S19.** Top, LC–$MS^3$ spectrum of $[M+H]^+$ of the sulfoxide of the Cys adduct of [$Dha^7$]MC-LR (**9c(O)**) at *m/z* 1118.0→981.1 (note, low signal-to-noise); bottom, LC–$MS^2$ spectrum of $[M+H]^+$ of [$Dha^7$]MC-LR (**9**) at *m/z* 981.1.

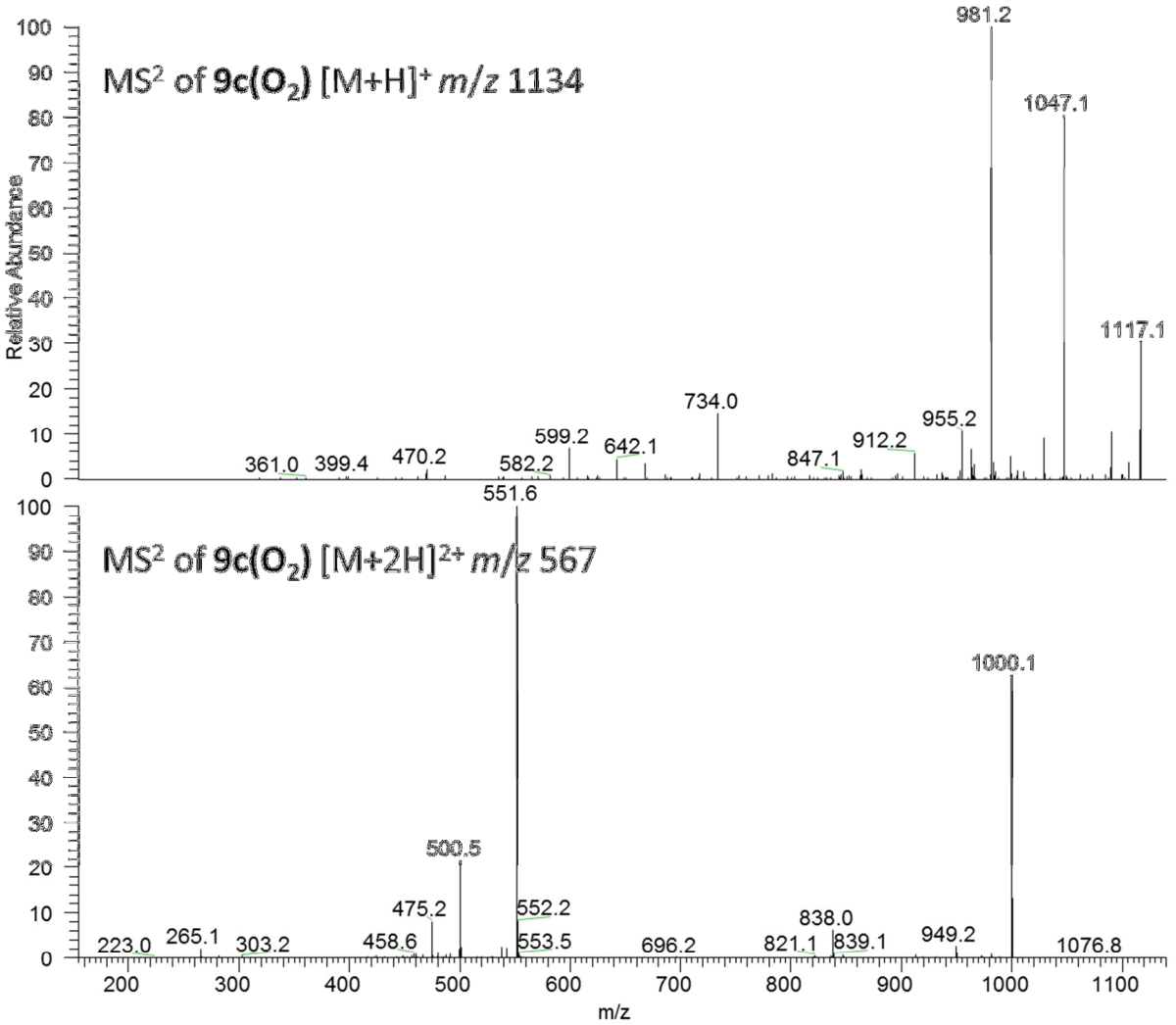


**Figure S20.** Top, LC–MS$^2$ spectrum of [M+H]$^+$ of the sulfone of the Cys adduct of [Dha$^7$]MC-LR (**9c(O$_2$)**) at *m/z* 1134.1; bottom, LC–MS$^2$ spectrum of [M+2H]$^{2+}$ of the sulfone of the Cys adduct of [Dha$^7$]MC-LR (**9c(O$_2$)**) at *m/z* 567.7.

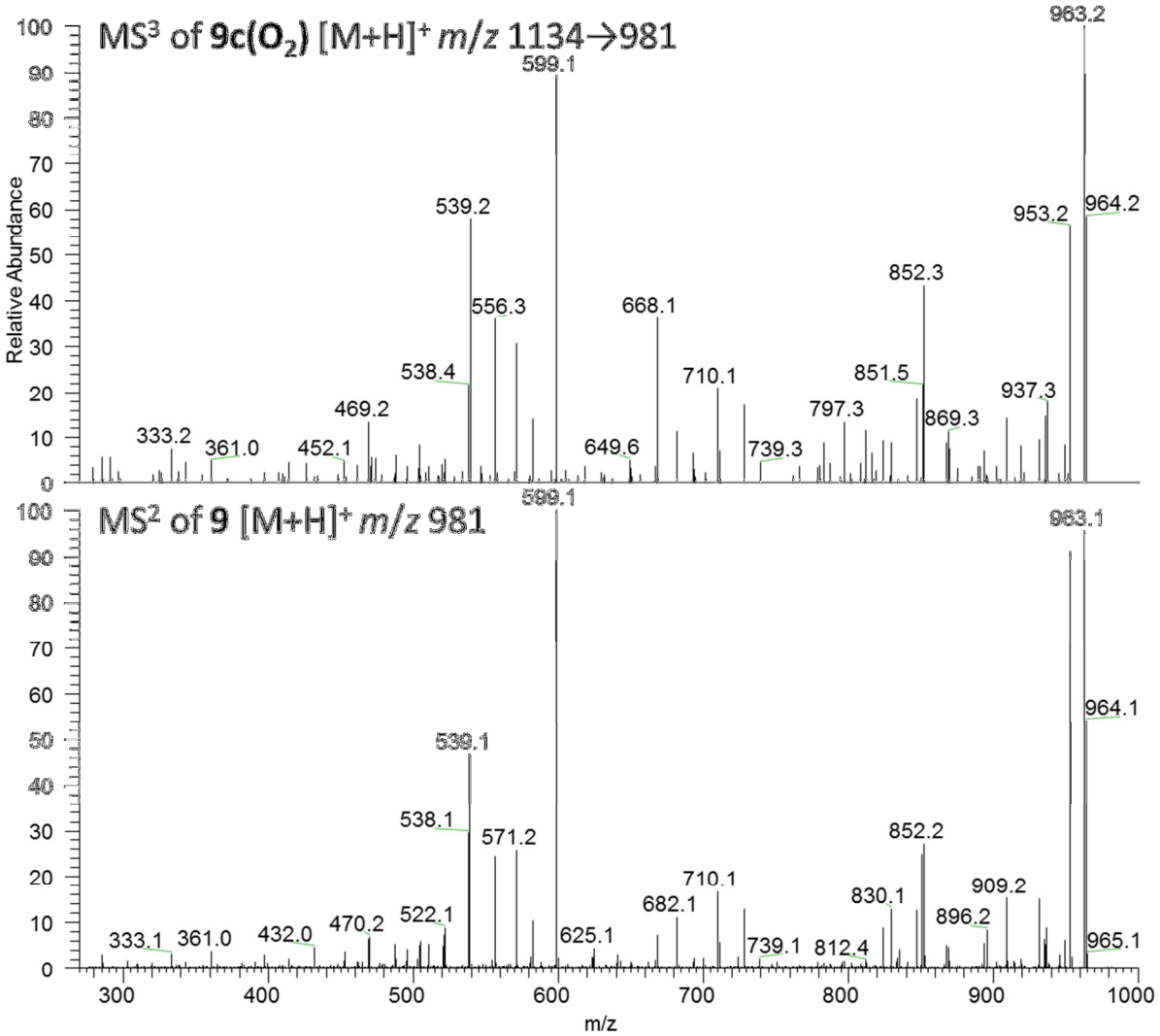


**Figure S21.** Top, LC–$MS^3$ spectrum of $[M+H]^+$ of the sulfone of the Cys adduct of [$Dha^7$]MC-LR (**9c($O_2$)**) at *m/z* 1134.1→981.1; bottom, LC–$MS^2$ spectrum of $[M+H]^+$ of [$Dha^7$]MC-LR (**9**) at *m/z* 981.1.

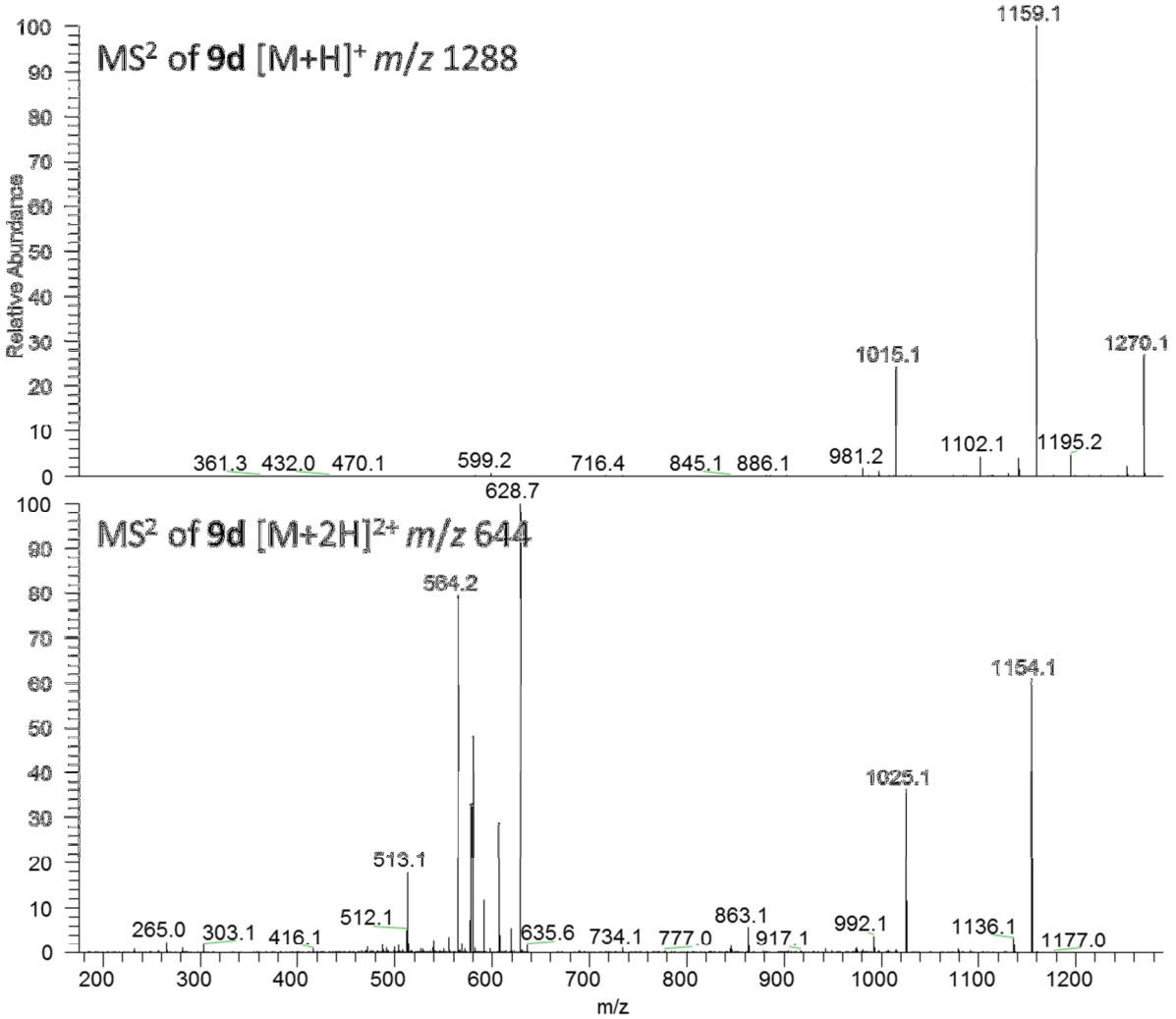


**Figure S22.** Top, LC–$MS^2$ spectrum of $[M+H]^+$ of the GSH adduct of [$Dha^7$]MC-LR (**9d**) at *m*/*z* 1288.1; bottom, LC–$MS^2$ spectrum of $[M+2H]^{2+}$ of the GSH adduct of [$Dha^7$]MC-LR (**9d**) at *m*/*z* 644.8.

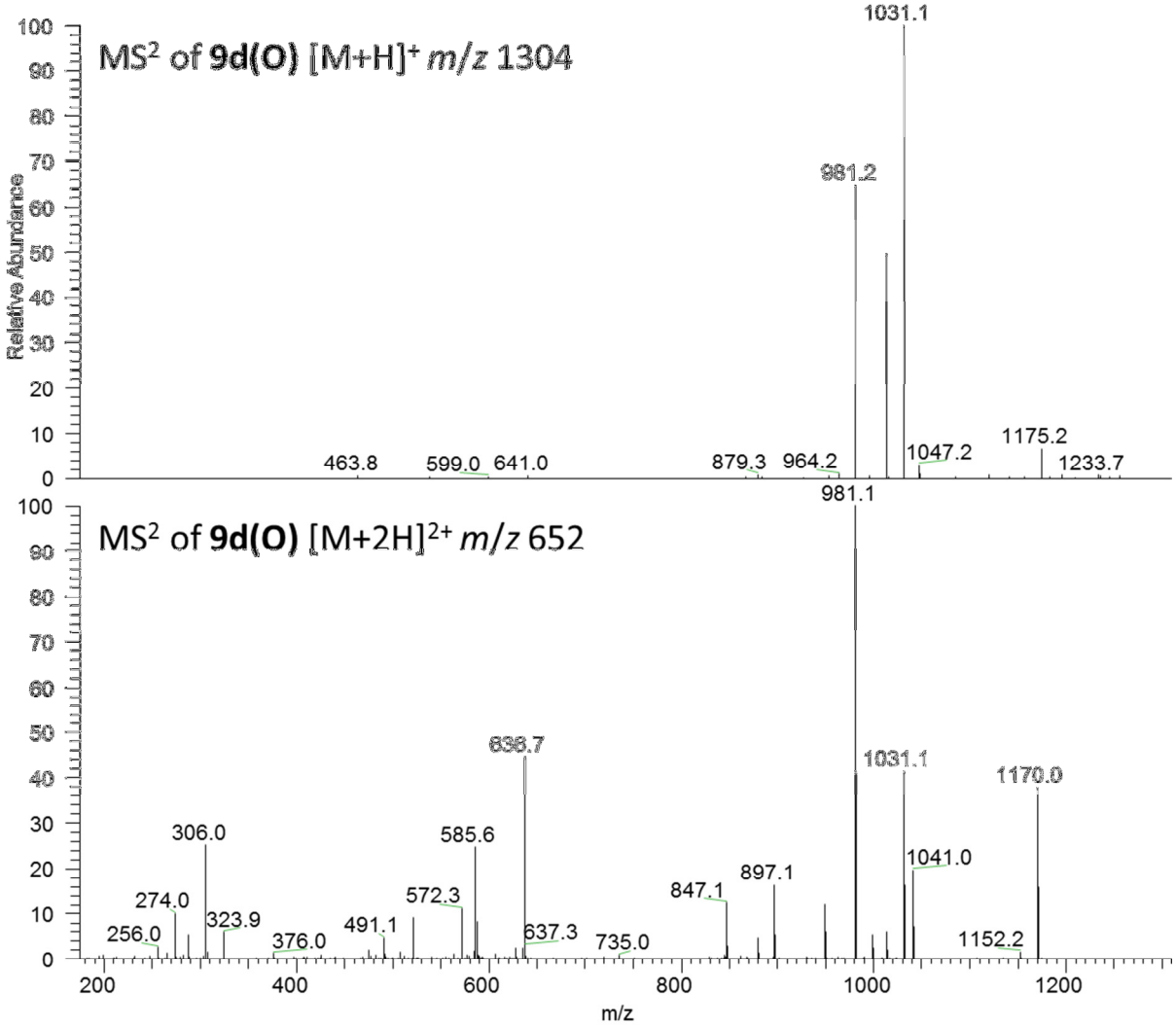


**Figure S23.** Top, LC–MS$^2$ spectrum of $[M+H]^+$ of the sulfoxide of the GSH adduct of [Dha$^7$]MC-LR (**9d(O)**) at *m*/*z* 1304.0; bottom, LC–MS$^2$ spectrum of $[M+2H]^{2+}$ of the sulfoxide of the GSH adduct of [Dha$^7$]MC-LR (**9d(O)**) at *m*/*z* 652.8.

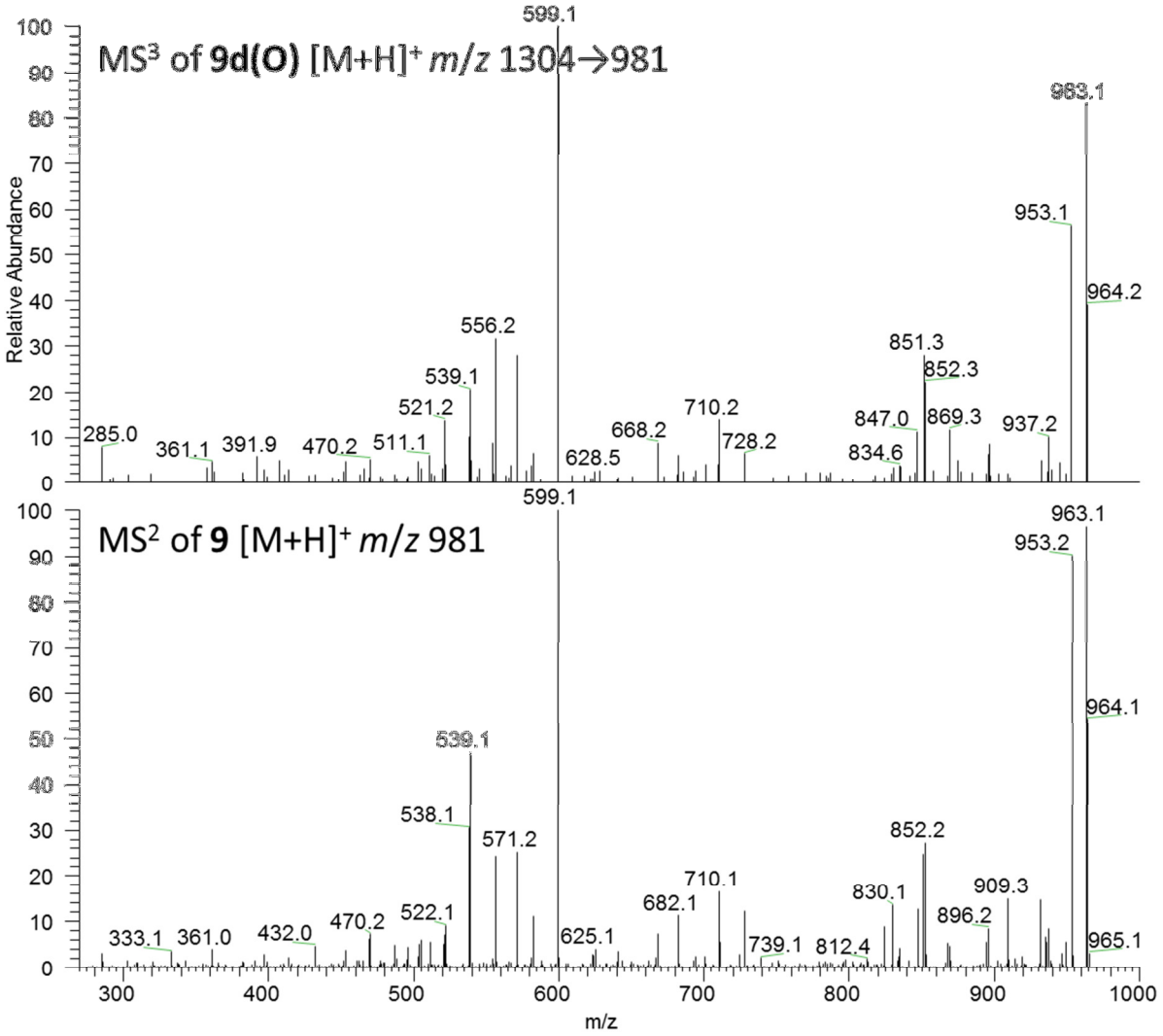


**Figure S24.** Top, LC–$MS^3$ spectrum of $[M+H]^+$ of the sulfoxide of the GSH adduct of [$Dha^7$]MC-LR (**9c(O)**) at *m/z* 1304.0→981.1; bottom, LC–$MS^2$ spectrum of $[M+H]^+$ of [$Dha^7$]MC-LR (**9**) at *m/z* 981.1.

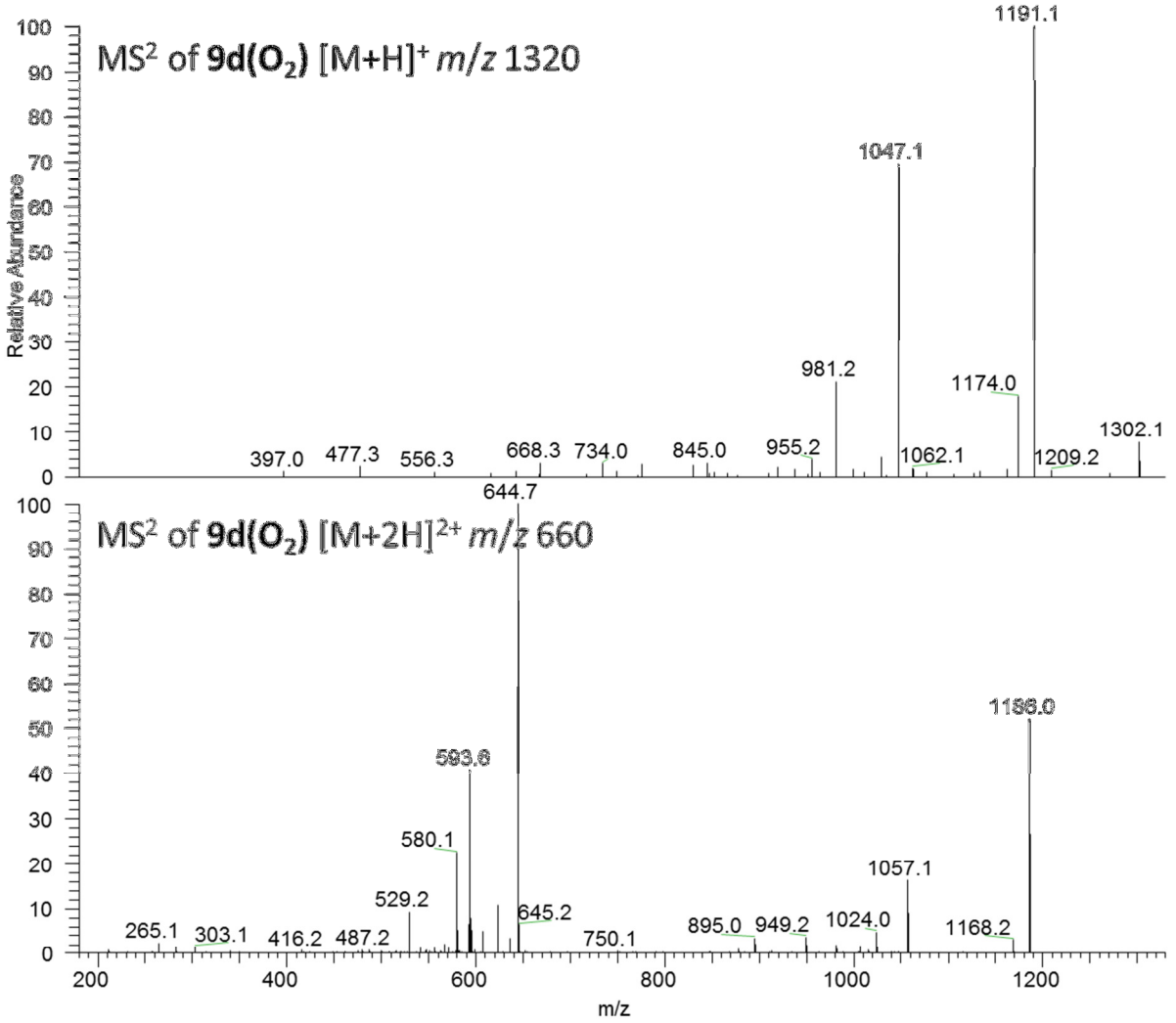


**Figure S25.** Top, LC–$MS^2$ spectrum of $[M+H]^+$ of the sulfone of the GSH adduct of [$Dha^7$]MC-LR (**9d($O_2$)**) at *m/z* 1320.1; bottom, LC–$MS^2$ spectrum of $[M+2H]^{2+}$ of the sulfone of the GSH adduct of [$Dha^7$]MC-LR (**9d($O_2$)**) at *m/z* 660.8.

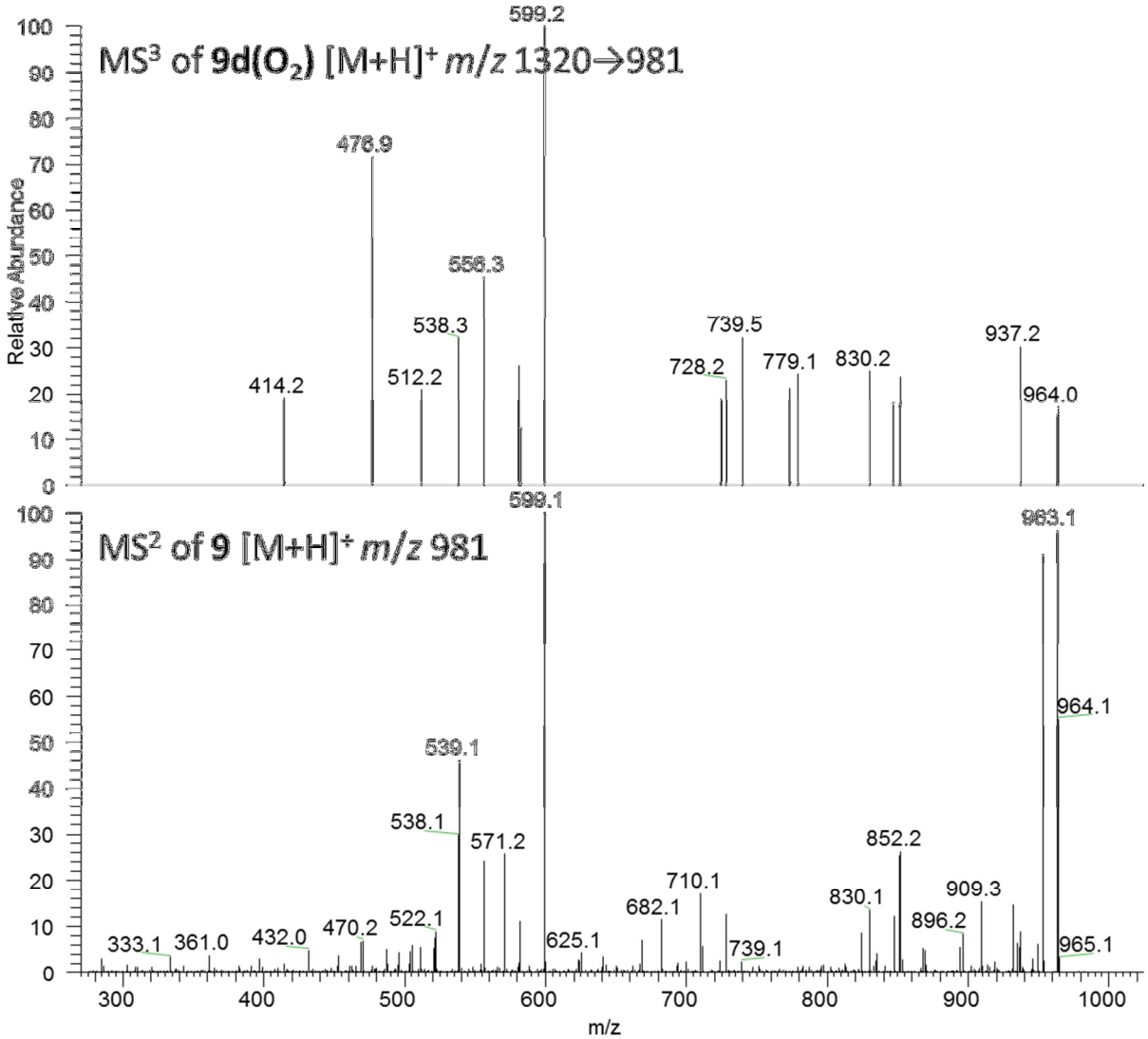


**Figure S26.** Top, LC–$MS^3$ spectrum of $[M+H]^+$ of the sulfone of the GSH adduct of [$Dha^7$]MC-LR (**9c($O_2$)**) at *m/z* 1320.1→981.5 (note, low signal-to-noise); bottom, LC–$MS^2$ spectrum of $[M+H]^+$ of [$Dha^7$]MC-LR (**9**) at *m/z* 981.1.

References

(1) Miles, C. O., Sandvik, M., Nonga, H. E., Ballot, A., Wilkins, A. L., Rise, F., Jaabæk, J. A. H., and Loader, J. I. (2016) Conjugation of microcystins with thiols is reversible: base-catalyzed deconjugation for chemical analysis. *Chem. Res. Toxicol. 29*, 860−870.